

Cross-correlation, triangulation, and curved-wavefront focusing of coral reef sound using a bi-linear hydrophone array

Simon E. Freeman^{a)}

American Society for Engineering Education, Washington, DC 20036

Michael J. Buckingham

Marine Physical Laboratory, Scripps Institution of Oceanography, University of California, San Diego, California 92093-0238

Lauren A. Freeman

National Research Council, Washington, DC 20001

Marc O. Lammers

Oceanwide Science Institute, Hawaii Institute of Marine Biology, Honolulu, Hawaii 96839

Gerald L. D'Spain

Marine Physical Laboratory, Scripps Institution of Oceanography, University of California, San Diego, California 92093-0238

(Received 15 May 2014; revised 3 October 2014; accepted 14 November 2014)

A seven element, bi-linear hydrophone array was deployed over a coral reef in the Papahānaumokuākea Marine National Monument, Northwest Hawaiian Islands, in order to investigate the spatial, temporal, and spectral properties of biological sound in an environment free of anthropogenic influences. Local biological sound sources, including snapping shrimp and other organisms, produced curved-wavefront acoustic arrivals at the array, allowing source location via focusing to be performed over an area of 1600 m². Initially, however, a rough estimate of source location was obtained from triangulation of pair-wise cross-correlations of the sound. Refinements to these initial source locations, and source frequency information, were then obtained using two techniques, conventional and adaptive focusing. It was found that most of the sources were situated on or inside the reef structure itself, rather than over adjacent sandy areas. Snapping-shrimp-like sounds, all with similar spectral characteristics, originated from individual sources predominantly in one area to the east of the array. To the west, the spectral and spatial distributions of the sources were more varied, suggesting the presence of a multitude of heterogeneous biological processes. In addition to the biological sounds, some low-frequency noise due to distant breaking waves was received from end-fire north of the array. © 2015 Acoustical Society of America.

[<http://dx.doi.org/10.1121/1.4904523>]

[BTH]

Pages: 30–41

I. INTRODUCTION

Tropical coral reef ecosystems provide habitat for a large variety of invertebrates, including snapping shrimp, hermit crabs, and sea urchins. Some of these animals are known to generate sound, the character of which varies from one type of organism to another. An individual snapping shrimp, for example, produces an extremely brief but very intense pulse of sound with a broad bandwidth, around 200 kHz or greater.¹ The physical mechanism responsible for such behavior is thought to be the collapse of a cavitation bubble, created by a high-speed water jet projected by the animal when it snaps shut its enlarged claw.² By way of contrast, sea urchins produce relatively narrow-band sound, in the range 800 to 2800 Hz, when sounds created by their feeding are amplified by the calcareous skeleton, or test, acting as a Helmholtz resonator.³

Although some of the properties of the sound produced by the inhabitants of the reef are known, many questions remain concerning the identity of the contributors to the reef soundscape and the mechanisms whereby the animals produce their characteristic acoustic signatures. Another largely unknown element is the ecologically relevant information that the reef sounds may contain.^{4–7,40} Such information includes the spatial distribution of biological sound sources over and around the reef, which, over time, can act as a gauge for the ecological state of the coral reef itself.

A single hydrophone (point receiver) is useful in providing the temporal and spectral characteristics of reef noise but, being omnidirectional, does not yield information on the directionality of the sound field or the locations of sound sources. Since the spatial distribution of reef organisms is known to be highly heterogeneous, the acoustic signature of the reef, as observed anywhere in the local vicinity, is expected to vary rapidly as a function of arrival angle. In order to retrieve the directionality of the sound field, the single point sensor must be replaced with an array of sensors, thereby forming an antenna having a directional response,

^{a)}Author to whom correspondence should be addressed. Electronic mail: simon.freeman@gmail.com

which can be used to map the locations of near-field sound sources.

Passive (receive-only) hydrophone arrays and their associated signal processing algorithms have been used extensively for the detection, localization, and tracking of marine mammals.^{8,9} In other areas of ecological monitoring and assessment the application of directional acoustic receivers has been limited,¹⁰⁻¹² although there is a growing interest in the use of passive (omnidirectional) underwater acoustic recording.^{6,13,14,40} The purpose of this article is to report on the use of an array of hydrophones to localize the acoustically active inhabitants of a pristine high-latitude coral reef ecosystem. In this case, “pristine” refers to a reef that is essentially undisturbed by anthropogenic activities and is free of anthropogenic noise.

During the summer of 2012, a bi-linear array of hydrophones was deployed next to a coral reef ecosystem near Kure Atoll in the Papahānaumokuākea Marine National Monument (PMNM), Northwestern Hawaiian Islands (NWHI). Initially, pair-wise cross-correlation between acoustic channels, combined with triangulation between hydrophone pairs, was used to obtain a crude estimate of the position (range and azimuth) of the sound sources on and around the reef. To refine these position estimates and to obtain the frequency characteristics of sources, array focusing on the curved wave fronts of the acoustic arrivals was performed using two techniques, conventional and adaptive processing.¹⁵ (Array focusing is similar to plane-wave beamforming except that the curvature of the wave fronts allows range as well as bearing to be estimated.) A two-dimensional map of sound sources was obtained, showing the distribution in a horizontal plane of the nearby acoustically active reef dwellers. An analysis of source localization errors, brought about by the correlated displacements of the hydrophones as ocean swells passed over the receiver station, is included in the discussion of the mapping procedure.

II. THE KURE ATOLL EXPERIMENT

Kure Atoll [Fig. 1(A)] became a state wildlife sanctuary in 1981 and was incorporated into the PMNM in 2006. Before its protection as a marine reserve, little fishing occurred at Kure Atoll due to its extremely remote location. Kure thus represents a present-day ecological baseline example of a high-latitude coral reef ecosystem that is free of anthropogenic noise. The experiment site was accessed via the National Oceanic and Atmospheric Administration (NOAA) Reef Assessment and Monitoring Program (RAMP) cruise HA-12-04. A hydrophone line array was deployed at a site on the southern outer reef at $28^{\circ}22.951'N$, $178^{\circ}19.484'W$ [Fig. 1(B)], where the water depth is 14.8 m and the seabed is composed of coralline sand. The array consisted of eleven elements arranged as four uniformly spaced sub-arrays (five elements each), with half-wavelength design frequencies increasing in octaves from 250 Hz to 2 kHz (corresponding to inter-element spacings of 0.325, 0.75, 1.5, and 3 m, respectively).

The array was deployed in an eroded spur-and-groove coral reef environment [Fig. 1(C)] in an obtuse angle, bi-linear configuration approximately 30 cm above the sea floor. The hydrophone cable and data acquisition electronics

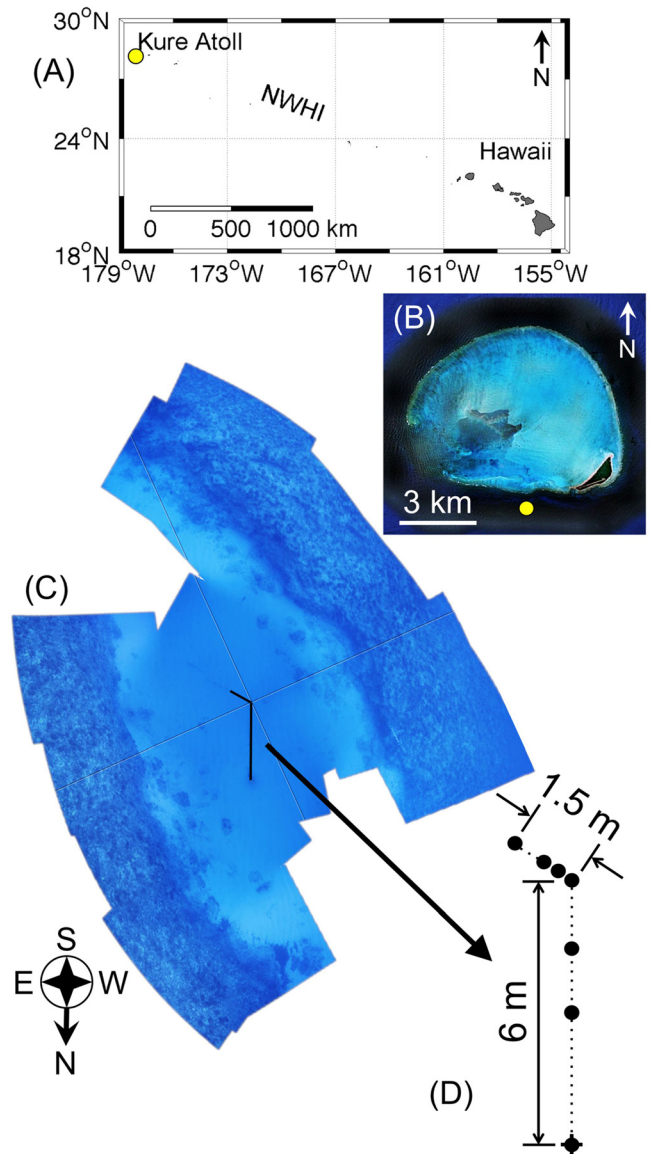


FIG. 1. (Color online) Chart and images of the array deployment site. (A) The relative position of Kure Atoll (filled circle) to the main Hawaiian Islands and the NWHI. (B) A satellite image of Kure Atoll. The filled circle indicates array position. The image is oriented such that north is at the top of the frame. (C) A bathymetric image mosaic showing the arrangement of the bi-linear array. The black lines indicate the position of the array cables. The primary axis of the array is oriented north-south as indicated by the compass rose on the lower right. (D) A close-up schematic of the array configuration and relative position of the hydrophone elements. The satellite image is courtesy of Google Earth.

were secured to the seafloor using sand anchors in the layout illustrated by Fig. 1(D). Anticipating that most of the biological sources of sound reside in and around the coral reef spurs, the array was oriented with its larger aperture aligned north-south, parallel to the spurs. While the array comprises of eleven hydrophones, only the seven identified in Fig. 1(D) were operational during the experiment.

During deployment, the water temperature was recorded at the array using portable underwater thermometers. Since the experiment location was completely exposed to open ocean currents, salinity was inferred from World Ocean Atlas data.¹⁶ Throughout the experiment the estimated sound

speed remained at 1531 ms^{-1} , as estimated from salinity and temperature data through the Mackenzie equation.¹⁷

Each hydrophone channel was sampled at $81.92 \text{ kSamples s}^{-1}$ with 24-bit resolution by a National Instruments PXI-8186 computer equipped with two PXI-4472 data acquisition boards, mounted in a pressure housing. A duty cycle recorded for four minutes continuously every half hour. The data were acquired using LABVIEW[®] 7.1 and processed in MATLAB[®] 2011b.

Douglas Sea State during the experiment was between 0 and 1, while swell state was 2 (a glass-calm sea over long-period swell). Consequently, open-ocean waves and weather-related noise were unlikely to have contributed to the recorded spectra. The hydrophone cable was secured with the greatest amount of line tension that could reasonably be exerted by a scuba diver. Nevertheless, some low-frequency cable strum was recorded due to Kure Atoll being circular in shape, offering relatively little protection against long-period ocean swell from any direction. To remove this noise, data were passed through a 512-point high-pass filter (corner frequency 100 Hz, stop frequency 500 Hz) after digitization. Cross-correlation and acoustic focusing were conducted within a horizontal, square area of 40 m by 40 m, centered at the array acoustic center (co-located with hydrophone #1). The survey area was discretized to 0.1 m resolution for both the processing of data collected *in situ* and the modeling of array performance.

III. ARRAY PERFORMANCE MODELING

Simulations of array performance, using array geometry identical to that used at sea, were conducted to estimate the range and azimuth based performance characteristics of the array. The directional performance characteristics of a line array and plane-wave beamforming system are often synoptically assessed through the beam pattern obtained by the broadside replica vector, per frequency. In this case, focusing involves the estimation of received level as a function of both azimuth and range, per frequency.

To ascertain the spatially dependent sensitivity of the array, the area encompassed by the main lobe surrounding each source location (analogous to the main lobe produced by a plane-wave beamformer) was quantified by the full area at half maximum (FAHM) envelope, analogous to the full width at half maximum concept used to quantify the main lobe width in plane-wave beamforming. Gaussian white noise sources were sequentially simulated around the survey area at 0.1 m increments. Conventional and white noise constrained focusing outputs were mapped as an ambiguity surface to show the spatial distribution of focusing accuracy. In order to investigate the change in array performance with decreasing wavelength, acoustic focusing outputs were calculated for frequency bins centered at 240 Hz, 2.4 kHz, 10 kHz, and 24 kHz.

A similar approach was employed to estimate the performance of the cross-correlation algorithm. However, rather than producing an estimate of the cross-correlation magnitude for a source at a given location, the accuracy of cross-correlation at each point was given by the size of the surrounding area that returned cross-correlation magnitudes over half maximum.

IV. ARRAY PROCESSING

The use of adaptive beamforming techniques greatly enhances spatial resolution and signal-to-noise ratio.¹⁸ However, these gains come at the cost of increased computational burden. Adaptive beamforming requires inversion of the cross-spectral density matrix (CSDM) on a per-frequency-bin basis. Furthermore, robust adaptive algorithms such as white noise constrained beamforming¹⁹ typically utilize an iterative approach to satisfy the white noise constraint, in which each iteration, per frequency bin, requires inversion of the CSDM.

Techniques such as Brent's method²⁰ can assist in minimizing the number of iterations. Developments that seek to mitigate the computational effort required in adaptive beamforming, such as dominant mode rejection, can improve the outcome in certain scenarios.^{21,22} Another method that reduces computational effort is to limit the range of the steering vectors to a sector most likely to contain the source of interest, the likelihood information being obtained *a priori*. This final method is utilized here.

A. Cross-correlation

If the geometric arrangement and sound speed between two time-synchronized, simultaneously recording hydrophones is known, an inverse Fourier transform of the coherence between these sensors provides an estimate of the sound field correlation.²³ When mapped to the axis between the two hydrophones, the relative azimuthal correlation is obtained. Using multiple hydrophone pairs that are not co-linear removes the axial ambiguity, allowing for localization of sound sources, via triangulation, in the near-field. Note that for a two-dimensional horizontal sensor arrangement, ambiguity remains in the vertical. Once source locations have been estimated, the focusing algorithm could then be restricted to these areas of interest.

The cross-spectral density of the ambient sound field, S , may be obtained using data from any two sensors (a, b). S is calculated in the frequency domain as the following:

$$S_{ab}(\omega) = \lim_{M \rightarrow \infty} \frac{1}{M} \sum_{i=1}^M X_a^i(\omega) X_b^{i*}(\omega), \quad (1)$$

where $X_a^i(\omega)$ represents the i th realization of the standard deviation at frequency ω for sensor a . An average is taken over M realizations of a sample period, T . $T \times f_s$, where f_s denotes the sampling frequency, is equivalent to the Fourier transform length in sample points.

For an accurate estimate of the cross-spectral density to be made, the sound field must be statistically stationary during the time required to obtain the ensemble average in Eq. (1). For recordings taken in dynamic acoustic environments, fewer averages and/or shorter Fourier transform lengths may approximate quasi-stationary conditions.

The cross-correlation function between two sensors is obtained by performing an inverse Fourier transform of the cross-spectral density, analogous to the Wiener-Khinchine theorem for autocorrelation:^{24,25}

$$\psi_{ab}(\tau) = \frac{1}{2\pi} \int_{-\infty}^{\infty} S_{ab}(\omega) e^{i\omega\tau} d\omega, \quad (2)$$

where τ is the correlation delay time. The maximum delay time, τ_d , between correlated arrivals at a sensor pair separated by distance d_{ab} is given by

$$\tau_d(ab) = \frac{d_{ab}}{c}. \quad (3)$$

Assuming plane-wave arrivals, ψ_{ab} may be mapped over look directions, θ , from $-\pi/2$ to $+\pi/2$ by $\theta = \sin^{-1} \tau/\tau_d$. Values that correspond to $|\tau/\tau_d| \leq 1$ represent the correlation of sounds arriving from an azimuthal window encompassing -90° to $+90^\circ$.

The number of data points within $|\tau/\tau_d| \leq 1$, referred to as m , is dependent upon the sampling frequency,

$$m_{ab} = 2\tau_d(ab)f_s, \quad (4)$$

where m is a whole integer, rounded downwards. Consequently, the resolution of ψ_{ab} between -90° to $+90^\circ$ is also proportional to the inter-element spacing. Interpolation in the time domain can be used to increase the temporal resolution. One way of efficiently performing this interpolation is through padding $S_{ab}(\omega)$ with zeros before obtaining $\psi_{ab}(\tau)$ as in Eq. (2).

In order to obtain the greatest number of independent cross-correlation estimates over the duration of the data set, the length of T should be chosen such that the number of samples per sampling period, $T \times f_s$, is as close to m as possible. In the case where $(T \times f_s) \geq m$, some of the cross-correlation values obtained in Eq. (2) will correspond to time delays greater than τ_d . In this case, the portion of T greater than m/f_s cannot be mapped to an azimuth with the approach used here and will remain unexamined. If $(T \times f_s) < m$, estimates of ψ will not extend the full azimuthal range.

Note that as with conventional delay-and-sum beamforming, mapping results in a nonlinear resolution in θ ,

$$\frac{d\tau_{ab}}{d\theta} = \tau_d(ab) \cos \theta. \quad (5)$$

The time delays corresponding to range, r , and azimuth, θ , coordinates from each hydrophone pair center are required for curved-wavefront cross-correlation and array focusing. The delay associated with any given location is obtained by calculating the time taken by sound waves originating at that location to travel the differential distance, ΔR , between the two sensors. For a given range and azimuth, $\Delta R(r, \theta)$ may be calculated trigonometrically,

$$\Delta R(r, \theta) = \sqrt{r^2 + \left(\frac{d_{ab}}{2}\right)^2 - rd \cos\left(\frac{\pi}{2} + \theta\right)} - \sqrt{r^2 + \left(\frac{d_{ab}}{2}\right)^2 - rd \cos\left(\frac{\pi}{2} - \theta\right)}, \quad (6)$$

and the delay time $\tau_{ab}(r, \theta)$ is inferred by dividing $\Delta R(r, \theta)$ by the estimated sound speed

$$\tau_{ab}(r, \theta) = \frac{\Delta R(r, \theta)}{c}. \quad (7)$$

The convention in this analysis is for positive delays when wavefronts arrive at sensor a before they arrive at b .

Correlation magnitudes for each pair of hydrophones were mapped to time delays calculated using Eq. (7) over a two-dimensional grid surrounding the array. Mapping resulted in ‘‘rays’’ of correlation magnitudes that curve outward from the aperture between each hydrophone pair. Triangulating rays from each sensor pair permitted the estimation of sound source positions over the array plane.

Using cross-correlation to determine source azimuth and location is a well-established technique. Ferguson²⁶ used a similar technique to that described above, but for the purpose of cross-correlating the beamformed outputs of two arrays. More recently, Ferguson and Cleary²⁷ used cross-correlation to estimate the positions of snapping shrimp. However, the use of a fast cross-correlation process to guide and restrict a more time-consuming acoustic focusing algorithm appears to be a novel method of suppressing noise and reducing computational burden.

B. Curved-wavefront focusing

For curved-wavefront acoustic focusing, steering vectors $D(\omega, \theta, r)$ of length N were calculated through a similar process to Eq. (7), except that the time delays for the hydrophone positions were calculated with respect to the array acoustic center [the northernmost hydrophone as shown in Fig. 1(D)]. In this case, ΔR is defined as the difference between r , the distance from a given location and the array center, and r_2, r_3, \dots, r_N , the distances between that location and the other hydrophones. The time delay vector, $[\tau_1, \tau_2, \dots, \tau_N]$, is thus calculated as follows:

$$[\tau_1, \tau_2, \dots, \tau_N](r, \theta) = \left[0, \frac{r - r_2}{c}, \frac{r - r_3}{c}, \dots, \frac{r - r_N}{c}\right]. \quad (8)$$

The phase delay/advance is then calculated in order to obtain the steering vector,

$$D(\omega, \theta, r) = e^{i\omega[\tau_1, \tau_2, \dots, \tau_N]}. \quad (9)$$

Using frequency-bin-centered vectors of length N , $B(\omega)$:

$$B(\omega) = [X_1(\omega)X_2(\omega) \cdots X_N(\omega)]. \quad (10)$$

Each estimate of the cross-spectral density matrix $R(\omega)$ is calculated as

$$R(\omega) = B(\omega)B^H(\omega), \quad (11)$$

in which the off-diagonal values of $R(\omega)$ are the cross-spectral densities described in Eq. (1). The superscript H denotes a complex conjugate (Hermitian) transpose operation. Consequently, acoustic focusing outputs and the correlation in the time-delay domain between every hydrophone can be acquired simultaneously.

Curved-wavefront acoustic focusing is implemented by applying steering vectors that are specific to an azimuth and range, $D(\omega, \theta, r)$, to $R(\omega)$ in a manner identical to plane-wave beamforming,¹⁵

$$P_{\text{conv}}(\omega, \theta, r) = D^H(\omega, \theta, r)R(\omega)D(\omega, \theta, r). \quad (12)$$

For white noise constrained acoustic focusing, the weighted steering vectors, w , are given by

$$w(\omega, \theta, r) = \frac{[R(\omega) + \varepsilon I]_{\text{inv}} D(\omega, \theta, r)}{D^H(\omega, \theta, r)[R(\omega) + \varepsilon I]_{\text{inv}} D(\omega, \theta, r)}, \quad (13)$$

where $[R(\omega) + \varepsilon I]_{\text{inv}}$ is the inverse cross-spectral density matrix, for which εI is a diagonal matrix of ε , a value iteratively calculated to satisfy minimum variance given the white noise constraint.¹⁵ The adaptive beamformer output is correspondingly,

$$P_{\text{WNC}}(\omega, \theta, r) = w^H(\omega, \theta, r)R(\omega)w(\omega, \theta, r). \quad (14)$$

V. DATA PROCESSING

A. Pressure spectral density estimates

Spectrograms and time-series plots were used to verify that recordings were free of clipping, electronic noise, or boat noise. A 1024-point fast-Fourier transform was applied to all channels simultaneously in 50% overlapped intervals with a Kaiser–Bessel window ($\alpha = 2.5$). Consequently, a seven-channel spectral estimate of the sound field was made every 6.3 ms. These spectral estimates were then applied to the cross-correlation and focusing algorithms described above.

B. Cross-correlation and acoustic focusing

Data used for cross-correlation processing were pre-whitened by dividing by the square root of the pressure spectral density and low-pass filtered using a 128-point finite impulse response (FIR) filter ($f_c = 20$ kHz, $f_s = 25$ kHz) to create a deterministic, gradual roll-off at higher frequencies.²⁸ In order to maintain an accurate estimate of the source spectra, data used by the focusing algorithms were not subject to the pre-whitening or filtering. A 7-by-7 CSDM was estimated for each frequency bin [Eq. (11)], and $N + 2$ CSDM estimates were averaged before cross-correlation and beamforming algorithms were implemented. An estimate of the sound field was thus created every 56.3 ms, more than sufficient in length to encompass the $500 \mu\text{s}$ duration of a typical snapping shrimp waveform.²⁹

Equation (2) was applied to the off-diagonal values in the CSDM in order to estimate the pair-wise cross-correlation between the array elements. With seven hydrophones, 21 geometrically unique pairs were available for triangulation. Cross-correlation vectors for each pair were limited to a time-delay range in which $|\tau_{ab}/\tau_{d(ab)}| \leq 1$, in order to map ψ_{ab} to azimuths from $+90^\circ$ to -90° , before interpolation over the surveyed area. These cross-correlation maps were then normalized by the maximum return in that particular time step before they were summed, and the locations of

cross-correlation maxima were recorded. The steering vectors [Eq. (9)] corresponding to these locations were subsequently applied to the averaged CSDM estimate through Eqs. (12)–(14), in order to obtain conventional and white noise constrained adaptive focusing outputs.

Although the white noise constraint is adjustable, only a single intermediate constraint of 8.5 dB down from conventional was utilized. An 8.5 dB constraint permits some “adaptiveness” and a substantial improvement in spatial resolution in the case of a plane-wave beamformer,³⁰ but retains sufficient robustness so that meaningful results may still be obtained without precise knowledge of array sensor positions.

VI. RESULTS

A. Model outputs

1. Cross-correlation performance

The accuracy of the cross-correlation algorithm over the surveyed area is shown in Fig. 2. The regions of highest accuracy were broadside to the longer arm of the bi-linear array (less than 2 m^2 per point source). Poorest performance (greater than 20 m^2 per point source) occurs end-fire to the longer arm of the array, furthest from the smaller arm, closest to the array’s northern extremity where inter-element spacing between hydrophones 1 and 2 was half the aperture of the arm (3 m).

2. Acoustic focusing performance

Maps showing the spatial variation of acoustic focusing performance for four frequencies and for both focusing

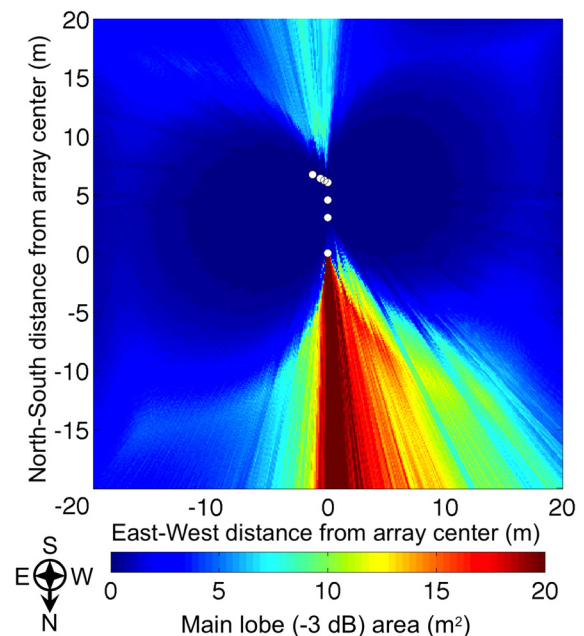


FIG. 2. (Color online) Simulated cross-correlation output displaying the localization accuracy of the cross-correlation algorithm. Broad-band sources were simulated sequentially at 0.1 m intervals and the area over which cross-correlation magnitude exceeded a given threshold was recorded. The scale bar indicates the FAHM (in m^2), a measure of the main lobe area of the received field for a source at each position. The white circles indicate hydrophone locations. The horizontal and vertical axes are oriented east-west and north-south, respectively. The compass rose indicates cardinal orientation.

techniques are presented in Fig. 3. The “focal pattern” produced by the spatially varying array sensitivity varies with wavelength, from a bimodal pattern at 240 Hz (with poorest performance closest to end-fire north) to a pattern severely influenced by aliasing at 24 kHz (the smallest inter-element spacing of the array was 0.375 m, a half-wavelength spacing corresponding to a frequency of 2 kHz). At mid-frequencies (from 2.4 to 10 kHz), focusing ability was reduced in the north-northwest quadrant within 10 m of hydrophone #1. This feature, combined with the relatively high FAHM values obtained in that region at other frequencies, suggests that the array suffered from poor broad-band performance close to end-fire north.

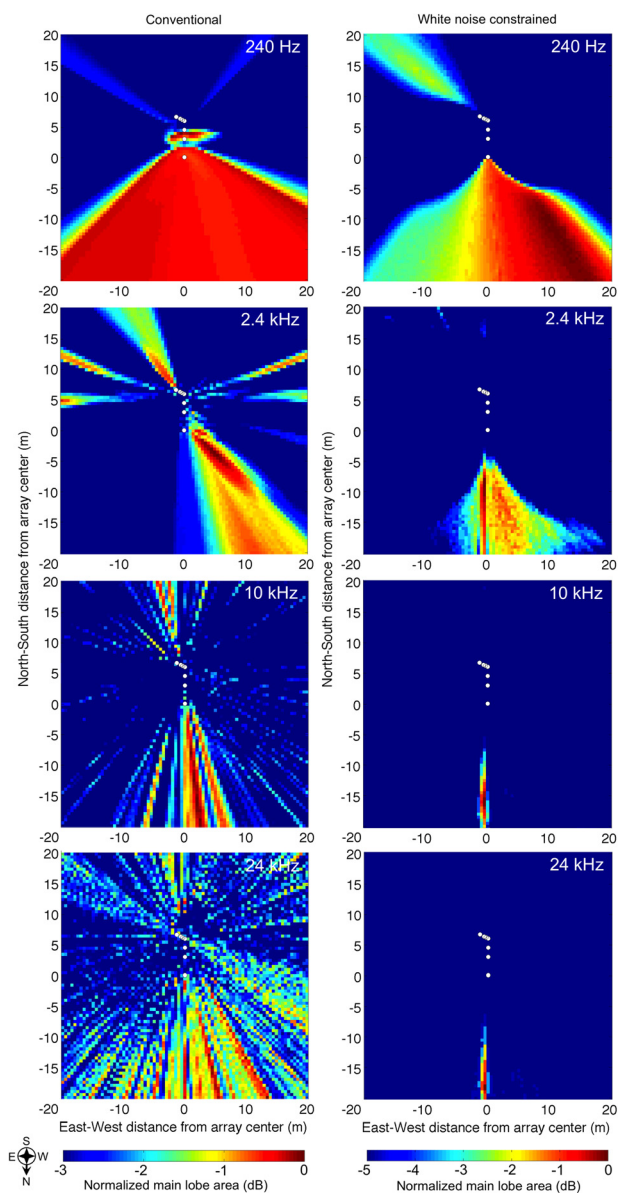


FIG. 3. (Color online) Normalized acoustic focusing outputs indicating the spatial variation in main lobe area using conventional array focusing (left column) and white noise constrained adaptive focusing (right column) for four frequencies: 240 Hz (top), 2.4 kHz, 10 kHz, and 24 kHz (bottom). The scale bar represents the normalized FAHM area (in dB) for a source at each position within the survey area, discretized to 0.1 m. The white circles indicate hydrophone sensor locations. The horizontal and vertical axes are oriented approximately east-west and north-south, respectively. The compass rose on the lower left indicates cardinal orientation.

B. Coral reef recordings

A four-minute recording was taken from 20:14 local time (sunset occurred at 18:48), when biological sound levels, and invertebrate activity, are generally higher than during the day.^{4,31} Figure 4(A) displays a spectrogram of the time-series recorded by hydrophone #1, while Fig. 4(B) displays the respective pressure spectral density estimate. The night-time underwater environment around Kure Atoll is dominated by mid-frequency sounds in the 3 to 27 kHz band. Although the averaged pressure spectra suggests a broad spectral peak centered between 6 to 15 kHz, the spectrogram reveals that much of the biological contribution to the soundscape originates from highly transient sounds of varying frequency content.

The spatial distribution of correlated sound sources was highly heterogeneous [Fig. 5(A)]. Correlated sound appears

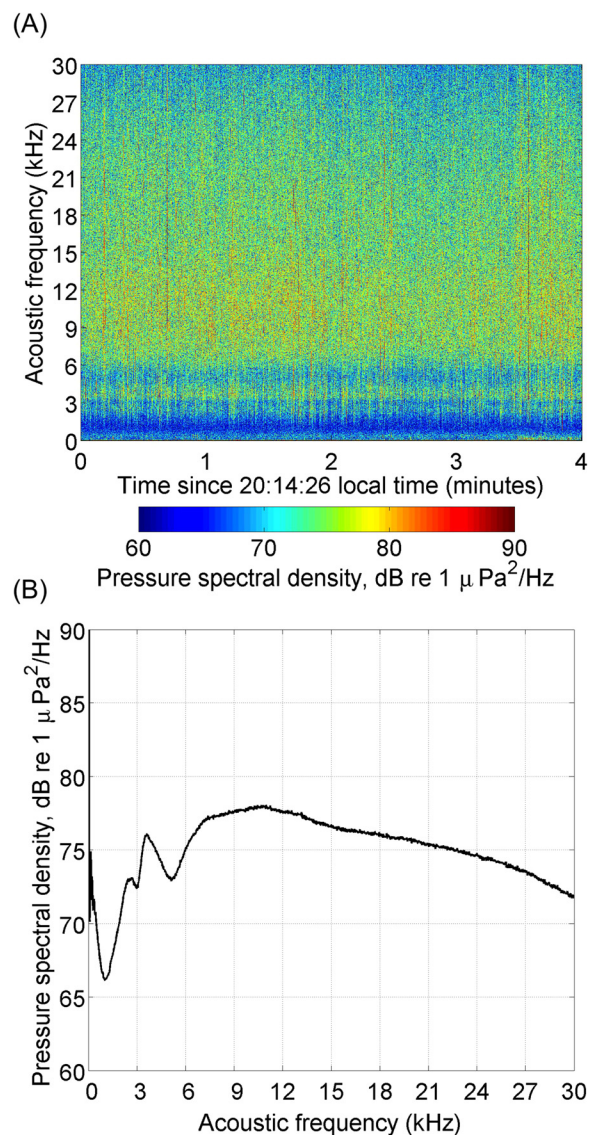


FIG. 4. (Color online) (A) A four-minute spectrogram and (B) pressure spectral density average recorded by hydrophone #1 of the array, from 20:14 local time at Kure Atoll. The spectrogram scale bar and the vertical axis of the pressure spectral density plot range between 60 to 90 dB re $1 \mu\text{Pa}^2/\text{Hz}$. The temporal and frequency resolutions of the spectrogram are 6.3 ms and 80 Hz, respectively. The low-frequency peak below 1 kHz is due to cable strum and flow noise.

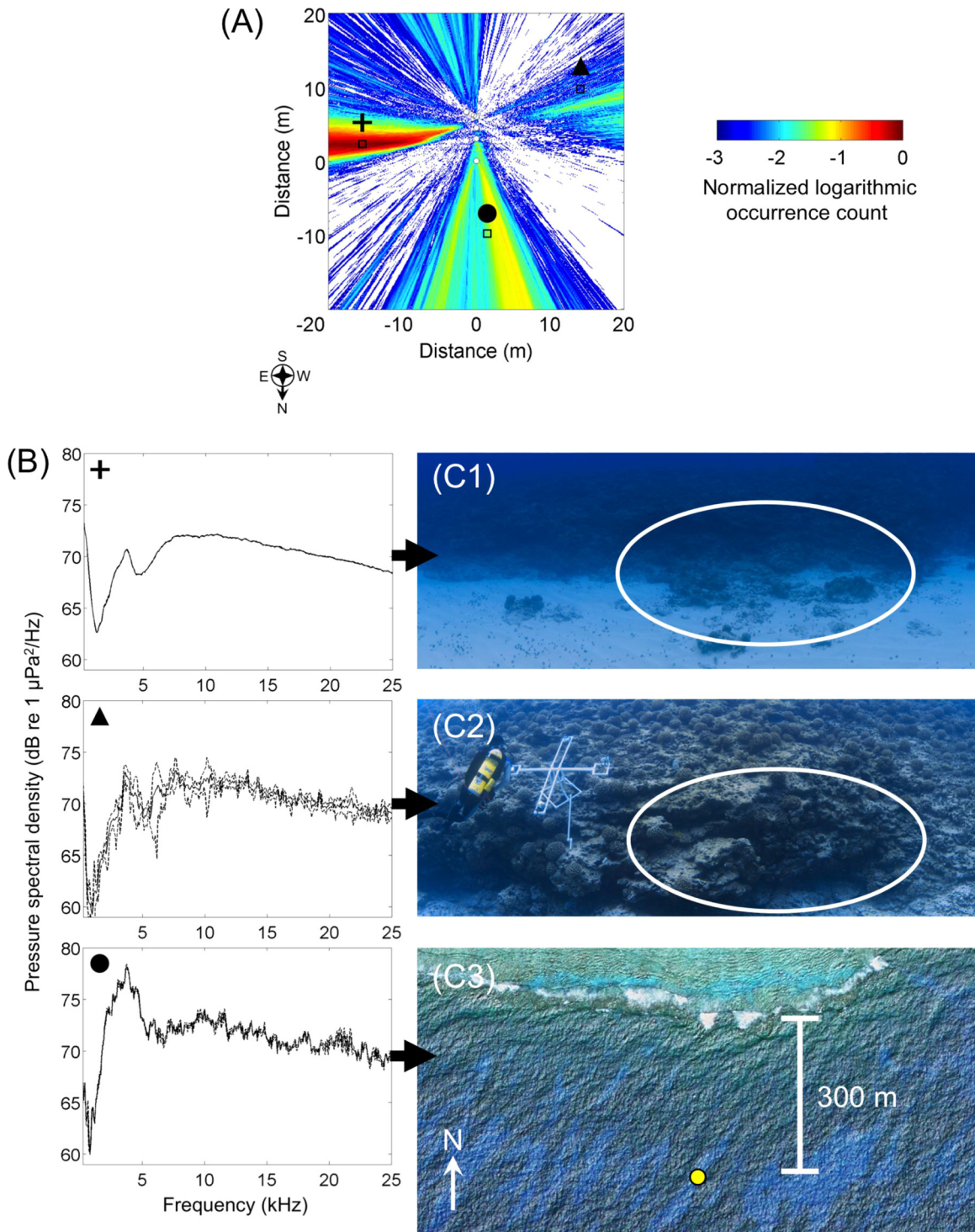


FIG. 5. (Color online) (A) The spatial distribution of cross-correlation magnitude values that exceeded the detection threshold over the recording shown in Fig. 4. The vertical axis represents distance north-south from the array center (north is toward the base of the figure, as per the compass rose on the lower left) and the horizontal axis represents distance east-west. A normalized logarithmic scale indicates the relative occurrence of highly correlated sounds over the survey area. For example, a source that exceeded the cross-correlation magnitude once within two minutes would return a value of -3.33 , while a constant loud source would return a value of zero. (B) Spatially averaged pressure spectral density estimates from three locations within the acoustic survey area. Pressure spectral density was averaged over each of the 1 m^2 areas as indicated by the unfilled black squares in (A). The symbols (cross, circle, and triangle) indicate the corresponding pressure spectral density plot. Solid lines show spectral estimate averages, while dashed lines indicate one standard deviation above and below each bin-centered mean. (C1) and (C2) Photographs taken from directly above the array acoustic center of the reef spurs to the west and east, respectively. The white ovals indicate the approximate area from which the spectral estimates in (B) were obtained. The diver and equipment visible in photograph (C2) were not present during recording. (C3) A satellite photograph of the field site and nearby reef break. The filled circle indicates the location of the array. The satellite image is courtesy of Google Earth.

to originate in three main areas: from an area directly east of the array about 10 m from the hydrophones, from a wide triangular area to the north of the array, and a spatially diffuse

area west of the array. The scarcity of correlated sound sources closer to the array corresponds with the extent of the sand channel between the reef spurs.

Example pressure spectral density estimates averaged over one-meter-square areas east, west, and north of the array are indicated in Fig. 5(B), while corresponding photographs of the associated source locations are shown in Fig. 5(C). The first two photographs [Figs. 5(C1) and 5(C2)] are photographs of the reef structure to the west and east of the array, respectively. The third photograph [Fig. 5(C3)] is a satellite image of the field site, showing the proximity of the nearby reef break.

Broad-band sources were observed in a region east of the array from about 5 m range, stronger and relatively uniform in pressure spectral density between 5 to 25 kHz when compared with sources to the west. To the north, sources that produced a strong low-frequency component (0–5 kHz) were apparent (Fig. 6). The sound sources in the area to the west were characterized by variable spectral peaks between

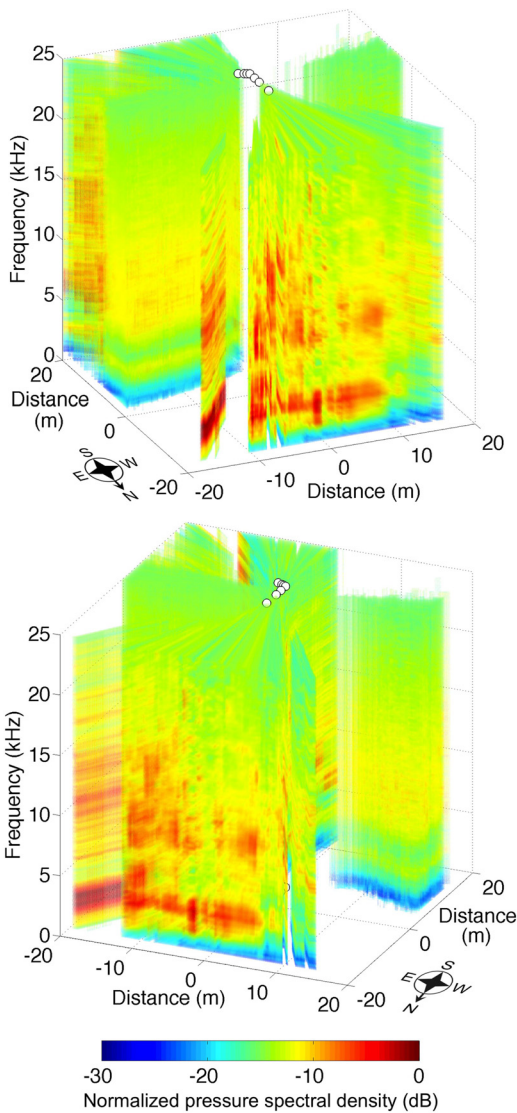


FIG. 6. (Color online) Two views of the same conventional acoustic focusing output over the four minutes of recording as shown in Fig. 4. The horizontal axes represent Cartesian distance from the array acoustic center, with cardinal directions indicated by the compass rose. The vertical axis represents acoustic frequency from 0 to 25 kHz. White circles on the 25 kHz plane represent the locations of the seven hydrophones. The scale bar represents normalized pressure spectral density in dB.

5 and 15 kHz, with most sounds exhibiting an 8 dB or greater decrease in pressure spectral density above 20 kHz, in comparison to the sources in the east (Fig. 7). Spectral density level appears relatively low below approximately 1 kHz. However, this observation may be due to the inability of the adaptive focusing algorithm to produce meaningful results at that frequency with the limited available aperture. The broad-band nature of sound from the area shown in Fig. 7(B) resulted in improved and more frequent instances of high cross-correlation, as seen in Fig. 5(A). Such characteristics resulted in the cross-correlation algorithm preferentially identifying these sound sources over comparatively narrow-band sounds from elsewhere.

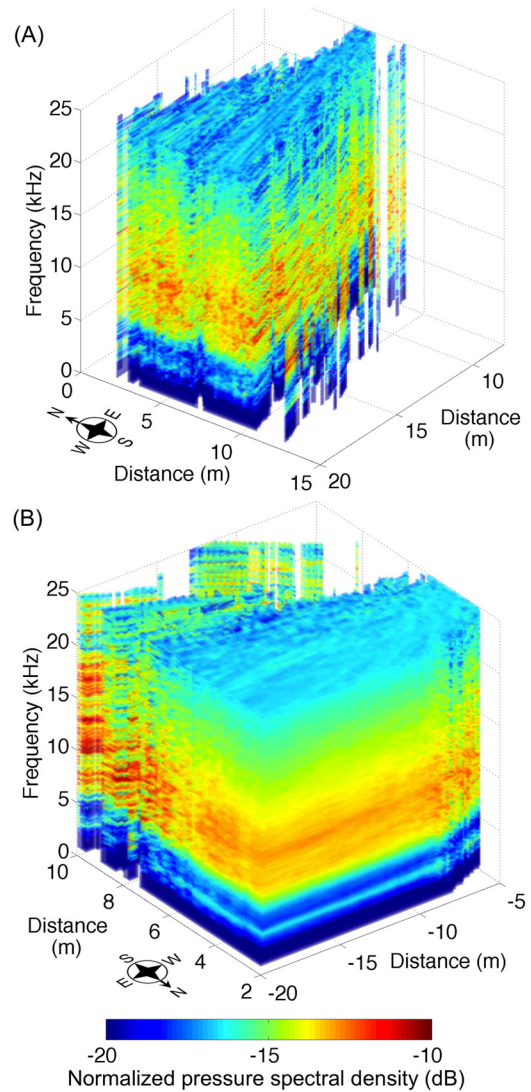


FIG. 7. (Color online) Two close-in images of sounds emanating from the two reef spurs either side of the array, obtained using white noise constrained acoustic focusing with an 8.5 dB constraint. (A) Pressure spectral densities from the reef spur directly west of the array, in which a number of small caverns were observed. (B) Pressure spectral densities from the rubble field east of the array, thought to encompass a colony of snapping shrimp. The horizontal axes indicate the Cartesian distance from the array acoustic center. The compass rose indicates cardinal orientation for each subfigure. The scale bar represents pressure spectral density, in dB, normalized to the highest level of pressure spectral density recorded over the entire survey area.

VII. DISCUSSION

A. Model outputs

The direction and range performance characteristics of the array and algorithms were estimated through modeling as no controlled acoustic sources were deployed for *in situ* performance validation. The simulated accuracy of the cross-correlation algorithm varied substantially with the location of the source. Accuracy was high in the regions near broadside to the primary axis of the array, while it was comparatively poor in the region near end-fire to the north of the array, as shown in Figs. 2 and 3. The spatial variation of focusing ability varied on a scale commensurate with the wavelength. Acoustic focusing outputs for both conventional and adaptive algorithms display the same general characteristics, although suppression of the more complicated lobe patterns at higher frequencies occurred in the adaptive case (Fig. 4).

While simulations show that aliasing and side lobes in the midfrequencies produced spurious source estimates, *a priori* knowledge of source locations can aid in identifying main lobes. With the cross-correlation algorithm limiting focusing to an area most likely to contain sources, the noise introduced by aliased and side lobes is reduced. While the frequency dependent sensitivity of the array is still an issue, a more accurate frequency representation of the sources is likely with such knowledge. A critical assumption here is that aliasing and side lobes from other, simultaneous sources do not substantially influence the frequency characteristics of each particular source of interest. For such influence to occur, the lobes created by one source must happen to be spatially coincident with the true location of another, simultaneous source. The likelihood of such an event occurring decreases with fewer simultaneous sources, the number of which is in turn is related to the time required to create each directional estimate. Thus, a higher sampling frequency is preferred, not only because oversampling is beneficial for filter design, but also because it reduces the probability of simultaneous detection by shortening the time required to create each CSDM estimate.

B. Coral reef recordings

The soundfield over a coral reef is dominated by broadband, highly transient biological sounds (Fig. 4). Over the relatively small area of the reef surveyed, substantial spatial variation in this sound was also observed (Figs. 5–7). In particular, the dominant sources of correlated sound appear to be concentrated approximately 10 to 20 m directly east of the array, adjacent to the nearby reef spur [Fig. 5(A)]. Figure 5(B) indicates that sounds from this area were homogeneous in frequency, characterized by a relatively flat spectrum between 5 and 25 kHz and a gentle roll-off above this band. The cross-correlation algorithm is more likely to return the highest magnitudes from areas where impulsive, broad-band sounds originate, which are more clearly correlated between channels. Consequently, it is likely that the algorithm preferentially detected sounds created by a colony of snapping shrimp in this area.^{2,30} However, the shrimp-like spectra still

show substantial deviation from what should be a fairly white spectral profile, assuming that snapping shrimp were the only source of sound from this region.^{1,32,33} It is possible that other biological sounds produced in the same area or close by have incoherently contributed, creating spectra that differ from that produced solely by snapping shrimp.⁴

Sounds arriving from the reef spur to the west are substantially more variable in frequency content than those from the east [Fig. 5(B)]. While it is almost certain that some snapping shrimp inhabit this area, the spectral heterogeneity strongly suggests that many additional acoustic processes, and by association different ecological processes, occur in this region. No visual, transect-style ecological survey was performed over the area. Given the cryptic and light-avoidance behavior of most benthic invertebrates, this technique would have been inadequate in estimating their abundance and diversity.

However, photographs were taken of the regions immediately surrounding the array [Fig. 5(C)]. To the west [Fig. 5(C1)], the coral reef bathymetry was more complex and included a number of small cave systems. The bathymetry to the east [Fig. 5(C2)] was comparatively plain, the dominant feature being a boulder field adjacent to a relatively smooth rock wall.

Inferences can be made from the structures seen in Figs. 5(C1) and 5(C2) regarding the organisms that inhabit these regions of the reef. Greater structural complexity is associated with a higher diversity of species, due to more protective habitat and increased surface area.³⁴ Several organisms known to be soniferous were observed in the caves to the west including fishes of the families *Pomacentridae*,^{35,36} *Holocentrinae* (or squirrelfish),³⁷ sea urchins of the genus *Evechinus*,³ and large numbers of spiny lobster, genus *Panulirus*.³⁸ Of these groups, only sea urchins were observed in the boulder field to the east. The fish families described here are known to produce sounds with a center frequency below 1 kHz. Consequently, their sounds were poorly resolved with the limited aperture used here. However, the cross-correlation technique is relatively frequency-independent. Results shown in Fig. 5 indicate that sounds originated from the region in which these fish were observed. Sounds produced by spiny lobster occupy a broader frequency band.³⁸ While their presence was also spatially correlated with the source locations of received sound, a higher level of acoustic focusing performance, in addition to concurrent visual confirmation, is required to causally link the received sounds with their sources. The presence of snapping shrimp in either area could not be visually confirmed as they spend the majority of their time out of sight. It should be noted that the spectral characteristics of the sounds produced by most marine organisms in the Hawaiian Islands are unknown, and identification of sound sources *in situ* requires further validation.

The recording of direct line-of-sight acoustic arrivals from sources on the reef flat (on top of the spur) was not possible due to the shadowing effect of the rocky structure. However, there were several sources of sound that likely contributed to the results shown from that area. A large number of invertebrates, at least some of which are known to produce sound, were observed within the cave system inside

the wall. As the edge of the rock spur in Figure (C2) was approximately 12 m from the hydrophone array, direct-path acoustic arrivals from these organisms were likely modified by their propagation through the porous rock. The relatively small array aperture in the east-west direction meant that the main lobe width in the vertical was fairly large. Consequently, the sensitivity of the array to sounds from above the array plane would have integrated sounds from that region with those produced by in-plane sources. It is also possible that sound from sources atop the reef spur propagated through the rocky bottom and scattered back into the water column from the edge of the rock spur. The compressional wave velocity in limestone bedrock is between 3 and 6 km s⁻¹ (Ref. 39) as compared to the estimated in-water sound speed of 1531 ms⁻¹. Consequently, sound waves that entered the rock atop the reef spur at any angle toward the array would have refracted further toward the edge of the rock spur. Similarly, as these sound waves re-enter the water from the rock spur, they would have refracted toward the horizontal.

Thus the sounds received at the array depicted as originating from beyond the rock wall are likely comprised of three components—sounds from organisms inside the porous rock, sound sources outside the survey plane but within the vertical envelope of the main lobe, and sub-bottom propagation of sound created atop the reef. To separate these sources, a three-dimensional array configuration and improved resolution in the vertical direction are required, in addition to more accurate estimates of sub-bottom sound propagation at the site.

Strong low-frequency sounds in the 0 to 5 kHz band were the dominant feature north of the array (Fig. 6). The origins of these sounds were less likely to be accurately estimated due to the poor performance in focusing near end-fire, particularly for lower frequencies (Figs. 2 and 3). The fan-like shape of source estimates in this area is clearly an artifact of insufficient aperture. In these regions, rays of high cross-correlation magnitude overlapped and produced diamond-shaped source location estimates. Figure 5(C3) shows the relative proximity of the southern reef break, where the low-frequency noise is likely to have originated. Because of the reef break noise, poor array performance, and the uncertainties indicated by array simulations, analysis was restricted to the areas near broadside, where focusing accuracy and resolution were highest.

White noise constrained focusing shows the contrast between the relatively uniform spectra to the east and the more diverse spectra to the west more clearly (Fig. 7). The spatial resolution shown in Fig. 7 suggests that for frequencies close to the design frequency of the array, the techniques described here are capable of identifying individual sound sources. However, verifying these sources requires geospatially referenced visual data, such as photographs or video, that are time-synchronized with array recordings.

C. Hydrophone location error

Although the array cable was secured tightly during deployment, divers observed slight movements of the cable

as long-period ocean swells (of approximately 15 to 20 s period) passed over the array. Visual observations indicated hydrophone movement to be on the order of 1 to 10 cm. The effect of this movement on the performance of the cross-correlation algorithm was estimated by simulating positioning errors when modeling the localization of a source at the approximate location of the suspected snapping shrimp colony.

Offsetting the position of the hydrophones along a catenary between the sand anchors approximated the observed *in situ* hydrophone displacement. Modeling was limited to the primary axis of the array (of 6 m aperture) as the secondary axis was relatively short (1.5 m).

The mean and standard deviation of bias (error between estimated and true location co-ordinates, Fig. 8, upper plot) remain relatively stationary for catenary offsets below 0.1 m, then increase asymmetrically depending on the direction the offset. Simultaneously, the area over which correlation is high decreases (Fig. 8, lower plot) as the magnitude of correlation between channels decreased. These results indicate that for small correlated hydrophone positioning errors (of less than 0.1 m), the effect on source location accuracy was within the error that accompanies estimations made using an accurately positioned array. In the case of more extreme correlated positioning errors, bias in estimates of range were generally larger than bias in estimates of azimuth.

An additional simulation of a source at the same location was conducted in which sound speed error was varied, rather than hydrophone position. The effect on the mean and standard deviation of the distance between the estimated and true source location (the “error distance”) was piecewise. As

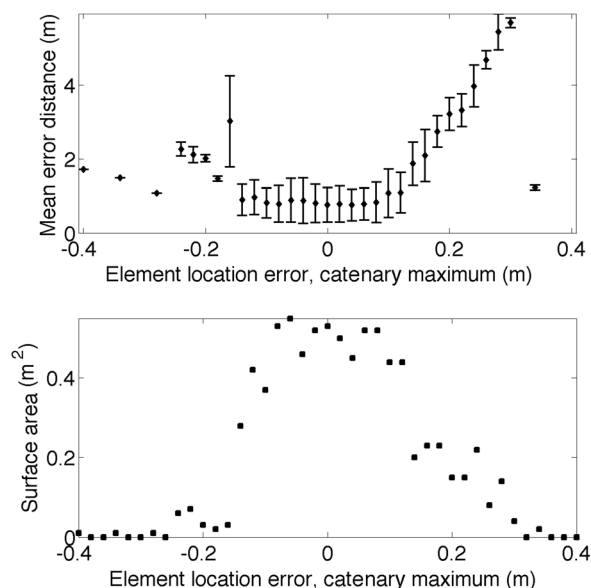


FIG. 8. The influence of correlated hydrophone array displacement in the shape of a catenary. The horizontal axis of both upper and lower plots indicate the maximum offset of the catenary (positive is in the west and southward directions). The simulated source location was 10 m to the east and 3 m to the south of the array center (i.e., in the approximate location of the snapping shrimp colony). The upper plot shows the spread of the error surface, i.e., the distance between points within the estimated source area and the true location. Error bars indicate one standard deviation. The lower plot indicates the size of the estimated surface area.

the magnitude of the sound speed error increased, the azimuth of cross-correlation rays varied to a point where rays no longer overlapped sufficiently to exceed the cross-correlation threshold, each time causing an increase in the error distance. The main lobe size varied in a manner that was more likely determined by the location of the source relative to the sensors. However, for the source position simulated here, the main lobe area varied by less than 6% over a $\pm 10 \text{ ms}^{-1}$ range from the sound speed that was estimated during the experiment (1531 ms^{-1}).

VIII. CONCLUSIONS

This study demonstrates the utility of a hydrophone array in spatially characterizing the ambient sound field over a coral reef, and provides an indication of the spatial scales over which the coral reef soundscape may vary. Coral reefs represent a highly heterogeneous acoustic environment in which a multitude of acoustically active organisms produce unique spectral signatures, in addition to sounds created by physical processes such as breaking waves. In order to reduce computational burden, a cross-correlation-based triangulation method identified the locations of sound sources that produced correlated arrivals at the array. Acoustic focusing, which requires greater computational resources, was then performed on these limited areas. Consequently, a spatial representation of the sound field was obtained that contained information originating only from the most correlated sources of sound.

Focusing using conventional and adaptive methods showed that ambiguity in source location estimates occurred to the north of the array near end-fire. Combined with the presence of a loud, low-frequency interferer in that direction (the reef break 300 m to the north), substantial low-frequency noise was introduced into focusing outputs. Evaluation of the sound field was thus restricted to areas close to broadside, to the east and west of the array.

Sounds from a broken boulder field located to the east of the array were consistent with a colony of snapping shrimp and dominated the sound field, although spectra from that area suggested other sounds may also have contributed from that region. The bathymetry was more built-up to the west, where a coral reef spur contained several small cave systems that offered a protective, overhanging habitat. In this area, sources of sound were more distributed in space and varied in frequency characteristics. A greater diversity and biomass of fauna were observed in this area, including soniferous animals such as lobster and sea urchins. However, the acoustic characteristics of these observed species have not been formally evaluated.

The passive techniques described here can be used to rapidly characterize the underwater acoustic environment in space, frequency characteristics, and time. The same techniques can suppress noise that may arrive from sources other than those of interest. In many shallow water environments the mid-frequency spectrum is dominated by biological sounds. Oftentimes, population information and the ecological impact of the organisms responsible for these sounds are difficult, if not impossible, to quantify through visual techniques.

Passive acoustic recording provides new information that is not subject to observational bias, the collection of which is not limited to periods in which natural light is available. Behavioral changes in reef organisms, such as those introduced when using video lighting at night, are not an issue.

The ambient sound field contains an enormous amount of information, and gaining useful and meaningful knowledge about the sources of sound is a challenging task. Not only are there a great many relevant sources of sound, the reverberant nature of shallow water areas and the complexity of the sea floor introduce bathymetry-related multipath arrivals and frequency-dependent attenuation. Determining the directionality and range of sound sources, and spatially filtering unrelated noise from the desired recordings, are important steps toward extracting ecologically relevant information from the ambient sound field.

ACKNOWLEDGMENTS

The authors would like to thank the staff at the Papahānaumokuākea Marine National Monument for their support and generosity on the HA-12-04 research cruise. This research was conducted under permit No. PMNM-2012-029. Carlie Wiener and Akiko Onuma provided public outreach and communication during the cruise. The authors would also like to thank students and staff at NOAA Pearl Harbor, in particular Scott Godwin and Jason Leonard, for their assistance with permitting and logistics during the cruise. The land-based assistance provided by Pollyanna Fisher-Pool was greatly appreciated. Dieter Bevans and Fernando Simonet at the Scripps Institution of Oceanography provided assistance with the hydrophone array. Finally, the authors would like to thank the captain and crew of the R/V Hi'ialakai for their assistance in deploying and retrieving sensor equipment. This work was supported by the Office of Naval Research (ONR) code 322OA, the University of California San Diego Academic Senate, and the National Science Foundation Integrative Graduate Education and Research Traineeship (IGERT) grant at the Scripps Institution of Oceanography.

¹D. H. Cato and M. J. Bell, "Ultrasonic ambient noise in Australian shallow waters at frequencies up to 200 kHz," Material Research Laboratory technical report No. MRL-TR91-23, Ascot Vale, Victoria (1992).

²M. Versluis, B. Schmitz, A. von der Heydt, and D. Lohse, "How snapping shrimp snap: Through cavitating bubbles," *Science* **289**, 2114–2117 (2000).

³C. Radford, A. Jeffs, C. T. Tindle, and J. C. Montgomery, "Resonating sea urchin skeletons create coastal choruses," *Mar. Ecol. Prog. Ser.* **362**, 37–43 (2008).

⁴S. E. Freeman, F. L. Rohwer, G. L. D'Spain, A. M. Friedlander, A. K. Gregg, S. A. Sandin, and M. J. Buckingham, "The origins of ambient biological sound from coral reef ecosystems in the Line Islands archipelago," *J. Acoust. Soc. Am.* **135**, 1775–1788 (2014).

⁵E. V. Kennedy, M. W. Holderied, J. M. Mair, H. M. Guzman, and S. D. Simpson, "Spatial patterns in reef-generated noise relate to habits and communities: Evidence from a Panamanian case study," *J. Exp. Mar. Biol. Ecol.* **395**, 85–92 (2010).

⁶R. A. Roundtree, R. G. Gilmore, C. A. Goudey, A. D. Hawkins, J. J. Luczkovich, and D. A. Mann, "Listening to fish: Applications of passive acoustics to fisheries science," *Fisheries* **31**, 433–446 (2006).

⁷S. Van Parijs and B. Southall, "Report of the 2006 NOAA national passive acoustics workshop: Developing a strategic program plan for NOAA's passive acoustics ocean observing system (PAOOS)," April 11–13, 2006,

- Woods Hole, Massachusetts, U. S. Dept. Commerce, NOAA Technical Memo No. NMFS-F/SPO 81 (2007).
- ⁸A. M. Thode, K. H. Kim, S. B. Blackwell, C. R. Greene, C. S. Nations, T. L. McDonald, and M. Macrander, "Automated detection and localization of bowhead whale sounds in the presence of seismic airgun surveys," *J. Acoust. Soc. Am.* **131**, 3726–3747 (2012).
- ⁹A. Thode, "Three-dimensional passive acoustic tracking of sperm whales (*Physeter macrocephalus*) in ray-refracting environments," *J. Acoust. Soc. Am.* **118**, 3575–3584 (2005).
- ¹⁰M. Chitre, S. Kuselan, and V. Pallayil, "Ambient noise imaging in warm shallow waters; robust statistical algorithms and range estimation," *J. Acoust. Soc. Am.* **132**, 838–847 (2012).
- ¹¹G. L. D'Spain and H. H. Batchelor, "Observations of biological choruses in the Southern California Bight: A chorus at midfrequencies," *J. Acoust. Soc. Am.* **120**, 1942–1955 (2006).
- ¹²D. W. Miklovic and M. T. Bird, "Snapping shrimp: Measuring their natural distribution in space and time with low frequency arrays," *IEEE Oceans* **4**, 2095–2099 (2001).
- ¹³J. R. Cotter, "The 'soundscape' of the sea, underwater navigation, and why we should be listening more," in *Advances in Fisheries Science: 50 Years on from Beverton and Holt* (Wiley-Blackwell, Oxford, 2008), pp. 451–471.
- ¹⁴M. O. Lammers, R. E. Brainard, W. W. L. Au, T. A. Mooney, and K. B. Wong, "An ecological acoustic recorder (EAR) for long-term monitoring of biological and anthropogenic sounds on coral reefs and other marine habitats," *J. Acoust. Soc. Am.* **123**, 1720–1728 (2008).
- ¹⁵D. J. DeFatta, J. G. Lucas, and W. S. Hodgkiss, *Digital Signal Processing* (Wiley, New York, 1988).
- ¹⁶J. I. Antonov, R. A. Locarini, T. P. Boyer, A. V. Mishonov, and H. E. Garcia, Salinity, Vol. 2 of "World Ocean Atlas 2005," NOAA Atlas NESDIS 62, U.S. Government Printing Office, Washington, DC (2006).
- ¹⁷K. V. Mackenzie, "Nine-term equation for sound speed in the oceans," *J. Acoust. Soc. Am.* **70**(3), 807–812 (1981).
- ¹⁸J. Capon, "High-resolution frequency-wavenumber spectrum analysis," *Proc. IEEE* **57**(8), 1408–1418 (1969).
- ¹⁹H. Cox, R. M. Zeskind, and M. M. Owen, "Robust adaptive beamforming," *IEEE Trans. Acoust., Speech, Signal Process.* **35**(10), 1365–1376 (1987).
- ²⁰R. P. Brent, *Algorithms for Minimization without Derivatives* (Prentice Hall, Englewood Cliffs, NJ, 1973), pp. 61–78.
- ²¹T. R. Messerschmitt and R. A. Gramann, "Evaluation of the dominant mode rejection beamformer using reduced integration times," *IEEE J. Ocean. Eng.* **22**(2), 385–392 (1997).
- ²²D. A. Abraham and N. L. Owsley, "Beamforming with dominant mode rejection," *Oceans'90 Conference Proceedings* (1990), pp. 470–475.
- ²³M. J. Buckingham, *Noise in Electronic Devices and Systems* (Ellis Horwood, West Sussex, 1983), pp. 47–49.
- ²⁴N. Wiener, "Generalized harmonic analysis," *Acta Math.* **55**, 117–258 (1930).
- ²⁵A. Khintchine, "Korrelationstheorie der stationären stochastischen Prozesse" ("Correlation theory of stationary stochastic processes"), *Math. Ann.* **109**(1), 604–615 (1934).
- ²⁶B. G. Ferguson, "Improved time-delay estimates of underwater acoustic signals using beamforming and prefiltering techniques," *IEEE J. Ocean. Eng.* **14**(3), 238–244 (1989).
- ²⁷B. G. Ferguson and J. L. Cleary, "In situ source level and source position estimates of biological transient signals produced by snapping shrimp in an underwater environment," *J. Acoust. Soc. Am.* **109**(6), 3031–3037 (2001).
- ²⁸M. J. Buckingham, "Cross-correlation in band-limited ocean ambient noise fields," *J. Acoust. Soc. Am.* **131**(4), 2643–2657 (2012).
- ²⁹W. W. Au and K. Banks, "The acoustics of the snapping shrimp *Synalpheus parneomeris* in Kaneohe Bay," *J. Acoust. Soc. Am.* **103**, 41–47 (1998).
- ³⁰S. E. Freeman, G. L. D'Spain, S. D. Lynch, R. A. Stephen, K. D. Heaney, J. J. Murray, A. B. Baggeroer, P. F. Worcester, M. A. Dziechiuch, and J. A. Mercer, "Estimating the horizontal and vertical direction-of-arrival of water-borne seismic signals in the northern Philippine Sea," *J. Acoust. Soc. Am.* **134**(4), 3282–3298 (2013).
- ³¹F. A. Everest, R. W. Young, and M. W. Johnson, "Acoustical characteristics of noise produced by snapping shrimp," *J. Acoust. Soc. Am.* **20**, 137–142 (1948).
- ³²B. N. Kim, J. Hahn, B. K. Choi, and B. C. Kim, "Snapping shrimp sound measured under laboratory conditions," *Jpn. J. Appl. Phys.* **49**(7), 1–4 (2010).
- ³³R. E. Knowlton and J. M. Moulton, "Sound production in snapping shrimps *Alpheus (Crangon)* and *Synalpheus*," *Bio. Bull.* **125**, 311–331 (1963).
- ³⁴P. Dustan, O. Doherty, and S. Pardede, "Digital reef rugosity estimates coral reef habitat complexity," *PLoS One* **8**(2), e57386 (2013).
- ³⁵K. P. Maruska, K. S. Boyle, L. R. Dewan, and T. C. Tricas, "Sound production and spectral hearing sensitivity in the Hawaiian sergeant damselfish, *Abudefduf abdominalis*," *J. Exp. Biol.* **210**, 3990–4004 (2007).
- ³⁶D. A. Mann and P. S. Lobel, "Passive acoustic detection of sounds produced by the damselfish, *Dascyllus albisella* (Pomacentridae)," *Bioacoustics* **6**(3), 199–213 (1995).
- ³⁷J. J. Luczkovich and M. Keusenkothen, "Behavior and sound production by Longspine Squirrelfish *Holocentrus rufus* during playback of predator and conspecific sounds," in *Proceedings of the American Academy of Underwater Sciences 26th Symposium*, Dauphin Island, AL (2007), pp. 127–134.
- ³⁸S. N. Patek, L. E. Shipp, and E. R. Staaterman, "The acoustics and acoustic behavior of the California spiny lobster (*Panulirus interruptus*)," *J. Acoust. Soc. Am.* **125**(5), 3434–3443 (2009).
- ³⁹L. E. Hamilton, "Sound velocity-density relations in sea-floor sediments and rocks," *J. Acoust. Soc. Am.* **63**(2), 366–377 (1978).
- ⁴⁰J. J. B. Piercy, E. A. Codling, A. J. Hill, D. J. Smith, and S. D. Simpson, "Habitat quality affects sound production and likely distance of detection on coral reefs," *Mar. Ecol. Prog. Ser.* **516**, 35–47 (2014).